ACS APPLIED POLYMER MATERIALS

pubs.acs.org/acsapm Article

Regiospecific Poly(ethylene-co-vinyl alcohol) by ROMP of 3-Acetoxycyclooctene and Postpolymerization Modification for Barrier Material Applications

Claire E. Dingwell and Marc A. Hillmyer*

Cite This: ACS Appl. Polym. Mater. 2023, 5, 1828−1836 Read Online

ACCESS | Metrics & More | Article Recommendations | Supporting Information

ABSTRACT: Ethylene vinyl alcohol (EVOH) is an oxygen barrier polymer used to prevent premature degradation of food, pharmaceuticals, and other products due to its semicrystallinity, strong intermolecular interactions, and consequently low free volume. EVOH is made using traditional free-radical copolymerization, which leads to little structural regularity. We utilized ring-opening metathesis polymerization (ROMP) to determine how regioregularity impacts the barrier properties of EVOH-related materials. A regioregular (head-to-tail) polymer was synthesized from ROMP of 3-acetoxycyclooctene, followed by hydrogenation and deacylation to give a linear, highly regioregular EVOH (PH3OHCOE) containing the equivalent of 75 mol % ethylene units. The same process was carried out with 5-acetoxycyclooctene, but the resulting polymer (PH5OHCOE) is regiorandom. Both polymers were compared to an industry benchmark, EVOH-44, containing 44 mol % ethylene units. After processing, differential scanning calorimetry showed that the semicrystalline PH3OHCOE had a higher melting temperature and enthalpy of melting compared to semicrystalline PH5OHCOE, indicating that PH3OHCOE is more crystalline. This was confirmed by wide-angle X-ray scattering (WAXS). WAXS, rheological studies, and polarized optical microscopy showed that PH3OHCOE has a more well-defined crystal structure, a higher degree of hydrogen-bonding between −OH groups, and a higher glass transition temperature compared to PH5OHCOE. These differences were also highlighted in their tensile behavior, where PH3OHCOE and EVOH-44 exhibited brittle failure compared to the ductile behavior observed for PH5OHCOE. Oxygen barrier testing demonstrated that regioregular PH3OHCOE had an oxygen permeability more than a factor of 3 lower than regiorandom PH5OHCOE but still higher than EVOH-44, while water barrier testing showed that PH3OHCOE had the lowest water permeability, more than 6 times lower than EVOH-44. These results highlight the importance of regioregularity on the barrier properties of EVOH-like materials and show that structural regularity can lower oxygen permeability while maintaining low water permeability at the low vinyl alcohol content.

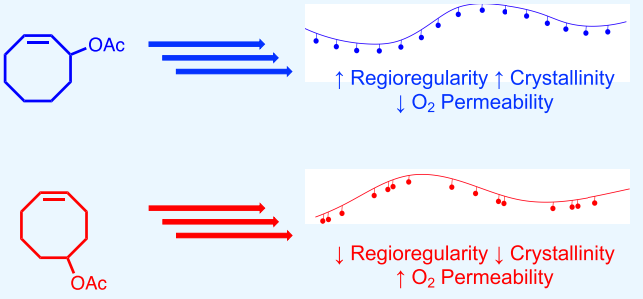

KEYWORDS: *functional polyolefins, gas barrier, metathesis, semicrystalline, packaging*

INTRODUCTION

Exposure of food[1] and pharmaceuticals[2] to oxygen can cause degradation to occur faster than their timescale for use. As such, oxygen barrier packaging materials are used to prevent early expiration, extend product lifetime, and avoid waste.[3] A widely used oxygen barrier material is termed ethylene vinyl alcohol (EVOH), a semicrystalline polyethylene (PE) and poly(vinyl alcohol) (PVOH) copolymer made by free-radical copolymerization of ethylene and vinyl acetate, followed by deacylation.[4] The microstructure is poorly controlled, and the polymers are branched as a result of this technique.[5] While PVOH homopolymer has better oxygen barrier properties than EVOH, PVOH has poor water barrier properties and is difficult to process due to low degradation temperatures.[6,7] In contrast, PE has high water barrier properties and good processability but poorer gas barrier properties.[8] Thus, incorporation of ethylene repeat units in EVOH improves moisture resistance, stability, and mechanical properties in this class of materials.[7] Even so, barrier packaging materials made with EVOH, usually containing 24−48 mol % ethylene units, typically require hydrophobic outer polyolefin layers in multilayer packaging.[9] When such EVOH compositions are placed in a humid environment, their oxygen permeability increases.[10,11]

Many structural characteristics affect polymer barrier properties. These can be best understood through the

Received: November 3, 2022
Accepted: January 30, 2023
Published: February 28, 2023

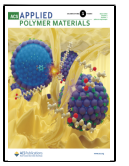

Scheme 1. ROMP of 3- and 5AcCOE, Followed by Hydrogenation and Deprotection to Give PH3- and PH5OHCOE[a33]

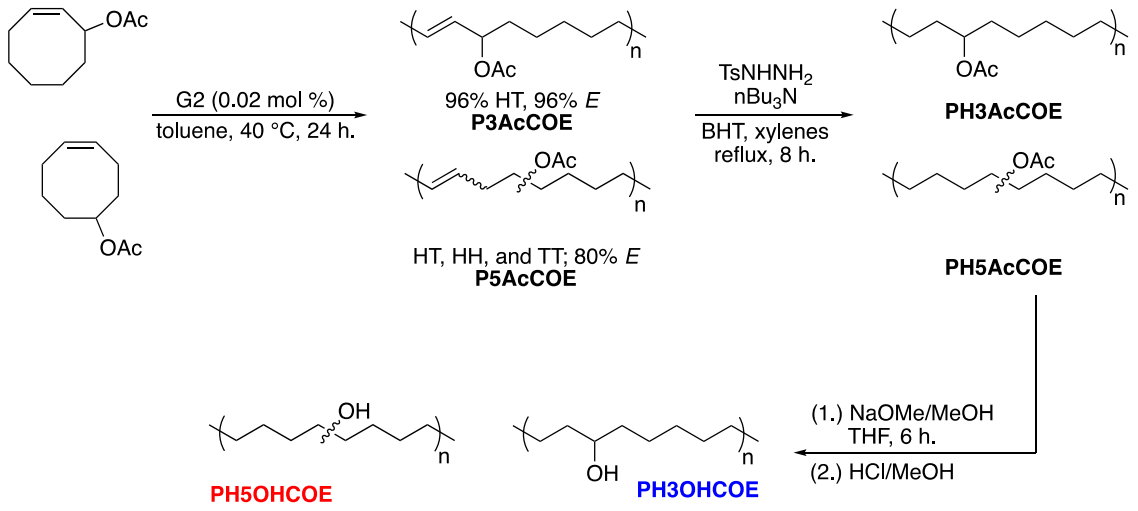

[a]Regioregularity and stereoregularity were calculated using ^{1}H NMR integrations of peak assignments made by Zhang et al.[33]

solution−diffusion theory of gas molecule permeation. First, the gas molecule must dissolve in the material, and then, it must diffuse through the material from one side to the other.[12,13] Oxygen is nonpolar and is poorly soluble in polar materials like EVOH.[14] Once dissolved, a gas molecule will diffuse preferentially through the amorphous phase of a semicrystalline polymer.[15,16] Therefore, an increasing degree of crystallinity (χ_c) nearly always improves barrier properties.[7,15,17] As for the amorphous phase in semicrystalline polymers, lower fractional free volume decreases oxygen diffusion.[18] Structural characteristics such as strong intermolecular interactions and high glass transition temperature (T_g) can improve barrier properties through decreases in fractional free volume.[15] These characteristics are also observed for EVOH due to its hydrogen-bonding hydroxyl groups along the backbone.[7] In EVOH, exposure to water causes its hydrogen-bonding groups to be disrupted by water molecules, decreasing intermolecular (i.e., polymer-polymer) interactions and T_g as a result of increasing free volume.[19]

Using a controlled polymerization method to synthesize EVOH-like materials could further improve barrier properties. Factors like χ_c and strength of intermolecular interactions are generally increased by structural regularity and decreased levels of branching.[20] Ring-opening metathesis polymerization (ROMP) allows for the controlled polymerization of cyclic alkenes, and the high functional group tolerance associated with ruthenium-catalyzed ROMP reactions allows monomers with polar functional groups to be polymerized.[21] ROMP of cyclic monomers like cyclooctene and cyclopentene also affords linear high-density polyethylene post-hydrogenation.[22] For example, Ramakrishnan and Chung[23] polymerized 5-diethylboranecyclooctene, followed by oxidation, to generate a regiorandom terpolymer of ethylene, vinyl alcohol, and butadiene. The resulting double bonds could also undergo hydroboration−oxidation to afford linear EVOH. Hillmyer et al.[24] utilized a direct approach to synthesize the same terpolymer through the polymerization of 5-hydroxycyclooctene. Ramakrishnan[25] also performed hydroboration−oxidation directly on poly(cyclooctene) to generate EVOH from ROMP. Scherman et al.[26] polymerized a *cis*- and *trans*-5,6-acetonidecyclooctene followed by hydrogenation and deprotection to give stereoregular EVOH with head-to-head (HH) hydroxyl groups. Scherman et al.[27] also polymerized a bicyclic cyclopentene monomer functionalized at the 3 and 5 positions with a cyclic silicon-protected diol by ROMP, followed by hydrogenation and deprotection, to give regioregular EVOH. Tuba et al.[28] studied ROMP of 3-hydroxycyclopentene without protecting groups; however, the resulting polymer had a low molar mass, and hydrogenation was not attempted on the ROMP-derived material. Very recently, Guillory et al.[29] reported stereo- and regioregular EVOH made by ROMP of 3-*tert*-butyldimethylsiloxycyclopentene and its enantiomerically pure derivatives. These polymers all displayed varying thermal properties due to their differing ethylene and vinyl alcohol concentrations, regio- and stereochemistry, and degrees of hydrogenation. In all cases, however, the oxygen or water barrier properties of these materials were not probed (polymer compositions summarized in Table S1).

The addition of substituents to the 3-position of cyclooctene gives regioregular head-to-tail (HT) polymers upon ROMP.[30,31] Martinez et al.[32] attribute this to unfavorable steric interactions between the substituent at the 3-position and the N-heterocyclic carbene ligand of the metathesis catalyst. Zhang et al.[33] then demonstrated that the polymerization of 3-acetoxycyclooctene (3AcCOE) is regioselective compared to the polymerization of 5-acetoxycyclooctene (5AcCOE). Upon hydrogenation, the resulting polymer derived from 3AcCOE showed crystallinity by differential scanning calorimetry (DSC) analysis, whereas that derived from 5AcCOE is amorphous. These vinyl acetate/ethylene (VAE) polymers are precursors to EVOH.[7] As regioregularity increases, χ_c should increase, as well as oxygen barrier properties of two compositionally identical polymers.

We aimed to investigate if, through control of structural regularity in this class of copolymers, we can achieve low oxygen permeability at lower levels of hydroxyl group incorporation along the backbone of the polymer as compared to typical EVOH materials. Improving oxygen permeability while maintaining water resistance can decrease the need for multilayer systems in barrier packaging, which require more energy to make, generate more waste, and are harder to recycle than single-layer films.[34] To this end, we synthesized regioregular poly(3-acetoxycyclooctene) (P3AcCOE) with high molar mass by ROMP, followed by hydrogenation to

https://doi.org/10.1021/acsapm.2c01918
ACS Appl. Polym. Mater. 2023, 5, 1828−1836

Table 1. Yield, Molar Mass, and Density Data for ROMP-Derived and Commercial Polymers

	isolated yield (%)	M_n (kg·mol^{-1})	M_w (kg·mol^{-1})	$Đ$	ρ (g·cm^{-3})[c]
P3AcCOE	53	351[a]	556[a]	1.6[a]	-
P5AcCOE	99	79[a]	119[a]	1.5[a]	-
PH3AcCOE	90	274[a]	439[a]	1.6[a]	-
PH5AcCOE	86	94[a]	152[a]	1.6[a]	-
PH3OHCOE	87	215[b]	772[b]	3.6[b]	1.15 ± 0.11[d]
PH5OHCOE	>99	78[b]	175[b]	2.3[b]	1.08 ± 0.01[d]
EVOH-44	-	26[b]	69[b]	2.6[b]	1.26 ± 0.05[e]

[a]Determined by THF-SEC (1.0 mL·min^{-1}, 25 °C) using MALS analysis. [b]Determined by HFIP-SEC (0.35 mL·min^{-1}, 40 °C) using PMMA standards. [c]Determined using a Mettler-Toledo scale according to Archimedes' principle. Measurement repeated three times per sample type, result presented as an average with standard deviation. [d]Determined from melt-processed films. [e]Determined from solvent-cast films.

remove backbone unsaturation. The resulting polymer was then deacylated under basic conditions to generate a linear ethylene vinyl alcohol polymer containing 75 mol % ethylene units. As a control, regiorandom poly(5-acetoxycyclooctene) (P5AcCOE) was also prepared by ROMP, followed by hydrogenation and deacylation. The resulting materials were solvent-cast into thin films and thermally annealed for thermal analysis, wide-angle X-ray scattering (WAXS), mechanical analysis, and barrier testing. Additionally, a commercial EVOH-44 copolymer with 44 mol % ethylene units was processed and analyzed alongside the polymers synthesized in this study as an industrially relevant benchmark.

RESULTS AND DISCUSSION

Ring-Opening Metathesis Polymerization. High molar mass P3AcCOE and P5AcCOE were synthesized based on literature procedures[33] (Scheme 1). Despite identical reaction conditions and catalyst loading, P3AcCOE had a lower isolated yield (53%), compared to that of P5AcCOE (99%). P3AcCOE also had a higher molar mass by size-exclusion chromatography (SEC) (Table 1). While P3AcCOE showed a number average molar mass (M_n) value by multi-angle light scattering (MALS) analysis of 351 kg·mol^{-1}, P5AcCOE exhibited an M_n of 79 kg·mol^{-1}. To determine the cause of these differences, monomer conversion studies were performed using proton nuclear magnetic resonance (^{1}H NMR) spectroscopy and size-exclusion chromatography (SEC). While the polymerization of 5AcCOE reached full conversion in 10 min, the polymerization of 3AcCOE only reached 87% conversion after 24 h (Figures S22−S24), which helps to explain the differences in isolated polymer yield. Additionally, the polymerization of 3AcCOE led to consistently increasing molar mass over time, while that of 5AcCOE initially showed increasing molar mass, followed by a decrease and plateau in molar mass (Figures S25−S28). Intramolecular cross-metathesis can result in an increase in putative cyclic oligomer content and a decrease in the resulting molar mass.[21,35] Upon analysis of the 24 h aliquots from the conversion studies by SEC, the P3AcCOE sample was estimated to have 4% cyclic oligomers, while the P5AcCOE level was estimated at 7% cyclic oligomers (Figures S29 and S30). Due to the steric hindrance of the reactive olefin by the OAc group in the 3-position, cross-metathesis reactions might occur less frequently in the P3AcCOE sample compared to the unhindered P5AcCOE sample. However, further loss of linear polymer likely occurred during polymer precipitation, as 7% of the polymer sample being attributed to cyclic oligomers would not be enough to account for the difference between conversion (87%) and yield (53%). Both had relatively low dispersity ($Đ$) values that were less than 2.

Regioregularity was determined by ^{1}H NMR analysis according to literature assignments.[33] P3AcCOE was determined to be 96% HT and 96% E, which compares well to results from previous studies.[30,33,36] P5AcCOE had no discernable peaks for HT, HH, or tail-to-tail (TT) protons in the ^{1}H NMR spectrum (Figure S3). Instead, the peaks appeared as a broad multiplet, indicating a regiorandom polymer. However, two multiplets can be discerned for E and Z arrangements of the backbone alkene (80% E). The differences in regiochemistry are especially prominent in the olefinic region of the ^{13}C NMR spectrum (Figure 1). While

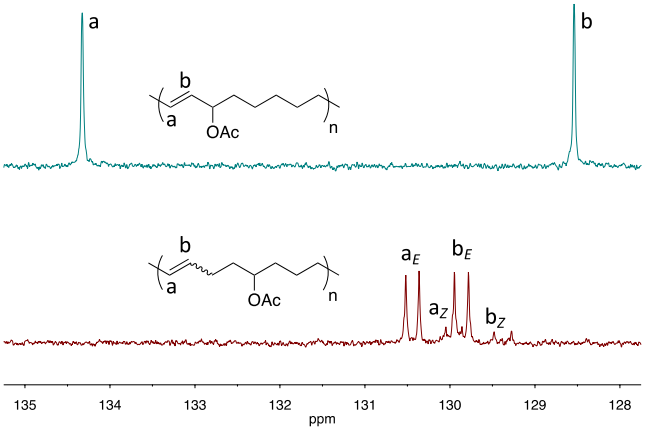

Figure 1. Olefinic region of the ^{13}C NMR spectrum in $CDCl_3$ for P3AcCOE (top, blue) and P5AcCOE (bottom, red).

only two peaks were observed for P3AcCOE for the HT/E microstructure, all eight possible peaks for HT/HH/TT and E/Z were observed for P5AcCOE.[24] This confirms the high regioregularity of P3AcCOE and the lack of regioregularity in P5AcCOE.

Hydrogenation and Deprotection. After polymerization, chemical hydrogenation was used to saturate the backbone olefins (Scheme 1). This reaction was achieved with high conversion (>99%) and high isolated yields (>85%) for both polymers. The molar mass differences were still present upon SEC analysis (Table 1). The M_n for the hydrogenated polymer, PH3AcCOE, decreased from 351 to 274 kg·mol^{-1} while retaining a low dispersity. The M_n for PH5AcCOE increased slightly as compared to the precursor to 94 kg·mol^{-1}. It is unclear why the molar mass decreased after hydrogenation of P3AcCOE. Following hydrogenation, deacylation was used to reveal hydroxyl groups along the backbone (Scheme 1). Sodium methoxide in methanol was added to the polymer in tetrahydrofuran (THF), followed by acidification with acidic

https://doi.org/10.1021/acsapm.2c01918
ACS Appl. Polym. Mater. 2023, 5, 1828−1836

methanol.[37] Fourier transform infrared (FT-IR) spectroscopy was used to characterize polymers before and after deacylation (Figure 2). Although NMR spectroscopy was also used to

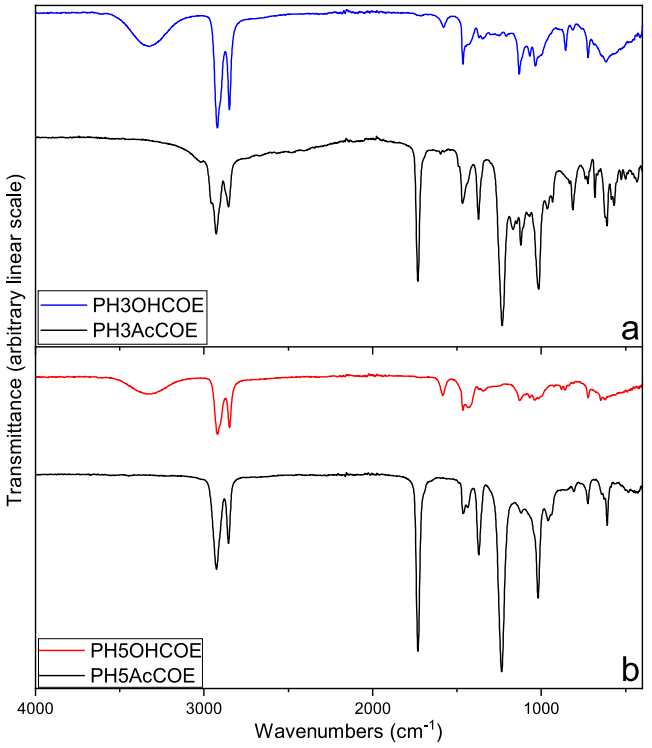

Figure 2. FT-IR spectra overlay before and after deprotection of (a) PH3AcCOE and (b) PH5AcCOE. Traces shifted vertically for clarity.

confirm polymer structure (Figures S13–S20), FT-IR more clearly showed changes in the backbone functional group. For reactions of both PH3AcCOE (Figure 2a) and PH5AcCOE (Figure 2b), an intense peak before the reaction can be seen at 1732 cm^{-1}, corresponding to the C═O stretch of the ester group. After the deacylation reaction, this peak is absent and a broad signal at 3332 cm^{-1} appeared, corresponding to −O−H stretches.

Post isolation, the resulting polymers (PH3OHCOE and PH5OHCOE) were white powders insoluble in most organic solvents. Characterization by SEC using hexafluoroisopropanol (HFIP) as the mobile phase was used to estimate molar mass (Table 1). The M_n for PH3OHCOE was measured to be 215 $kg{\cdot}mol^{-1}$ relative to PMMA standards. The dispersity also increased to 3.6. Although MALS may slightly overestimate M_n and underestimate dispersity, the large difference in dispersity could be due to polymer interaction with the column, which was supported by an unfortunate increase in column pressure following the measurement. A similar trend, although to a lesser extent, was observed for PH5OHCOE. The relative M_n for PH5OHCOE was 78 $kg{\cdot}mol^{-1}$, and the dispersity was 2.3. The ROMP-derived polymers were also compared to a commercial polymer, EVOH-44 (44 mol % ethylene), with a M_n of 26 $kg{\cdot}mol^{-1}$ using the same technique. A polymer with 75 mol % ethylene content to match the ROMP-derived polymers in this study was not readily available since lower vinyl alcohol content polymers prepared by radical polymerization methods typically lead to poor oxygen barrier properties and thus are not as practically useful.[18] The densities of these samples were measured by the Archimedes' principle (Table 1). EVOH-44 was found to have the highest density, followed by PH3OHCOE, then PH5OHCOE. This preliminarily suggests that EVOH-44 has a higher χ_c or a lower free volume with more tightly packed chains compared to PH3OHCOE, followed by PH5OHCOE.[38]

Thermal Characterization. DSC was used to investigate the thermal transitions in PH3OHCOE, PH5OHCOE, and EVOH-44. Analysis was performed on thin films made by drop-casting from HFIP, followed by annealing the films at 85 °C for 2 h. Figure 3a shows the first heating cycle after this

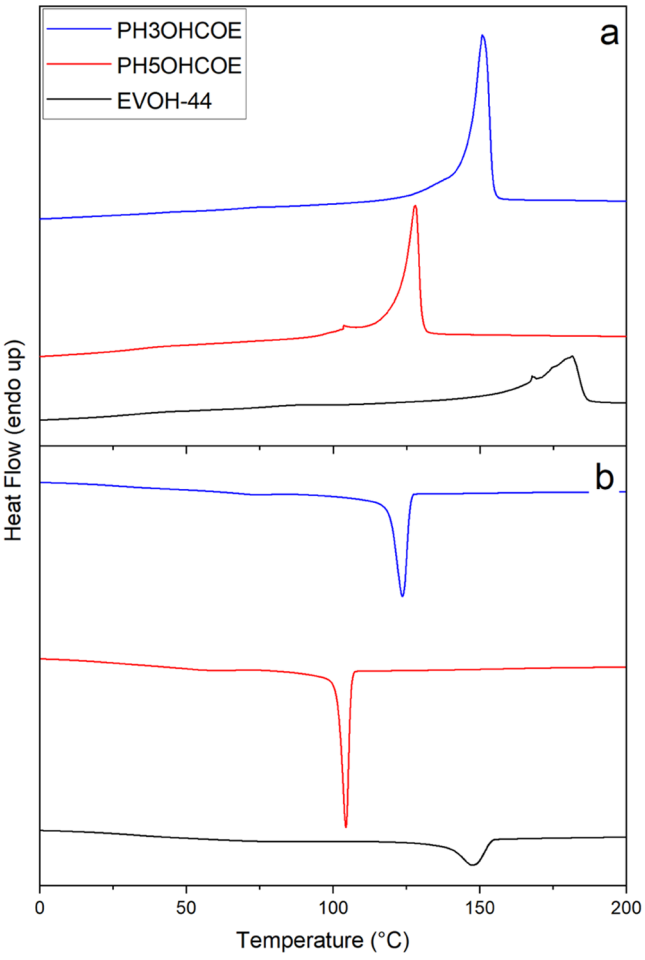

Figure 3. DSC traces with (a) first heating cycle (10 $°C{\cdot}min^{-1}$) and (b) first cooling cycle (10 $°C{\cdot}min^{-1}$) of solvent-cast thin films. Traces shifted vertically for clarity.

annealing step for PH3OHCOE, PH5OHCOE, and EVOH-44; Figure 3b shows the first cooling cycle and summarizes the results. No clear T_g was observed in the DSC trace of the solvent-cast polymers. PH5OHCOE has a lower melting temperature (T_m) of 128 °C and a lower enthalpy of melting (ΔH_m) of 81 $J{\cdot}g^{-1}$ compared to PH3OHCOE (151 °C and 113 $J{\cdot}g^{-1}$, respectively) after this thermal history. EVOH-44 had a higher T_m of 181 °C due to its lower ethylene content, but a lower ΔH_m of 70 $J{\cdot}g^{-1}$ compared to the ROMP-derived polymers. These values were used to estimate χ_c (Table 2); PH3OHCOE showed the highest χ_c, followed by EVOH-44, then PH5OHCOE.

Changes in molar mass can also result in changes of χ_c, although typically at much lower molar masses than those used in this study.[39] Thus, to explore the origins of the differences in

https://doi.org/10.1021/acsapm.2c01918
ACS Appl. Polym. Mater. 2023, 5, 1828−1836

Table 2. Thermal Transitions from TGA, DSC, DMTA, and Crystallinity Data from WAXS of PHOHCOE Polymers and EVOH-44

	EVOH-44	PH5OHCOE	PH3OHCOE
T_d (°C)[a]	331	419	418
T_m (°C)[b]	181	128	151
ΔH_m (J·g^{-1})[b]	70	81	113
T_c (°C)[c]	148	104	124
ΔH_c (J·g^{-1})[c]	32	66	66
χ_c (%)[d]	34	33	46
χ_c (%)[e]	36	43	46
T_g (°C)[f]	40	45	82
T_g (°C)[g]	93	94	96

[a]Determined by TGA at 5% mass loss in N_2 (10 °C·min^{-1}). [b]Determined by DSC of solvent-cast film from the first heating cycle (10 °C·min^{-1}). [c]Determined by DSC of solvent-cast film from the first cooling cycle (10 °C·min^{-1}). [d]Calculated from ΔH_m [χ_c = ($\Delta H_m/\Delta H_{f(100)}$)·100]. $\Delta H_{f(100)}$ (enthalpy of fusion for a 100% crystalline polymer) was calculated for each polymer type based on weight fraction (w) and literature $\Delta H_{f(100)}$ values[42] [$\Delta H_{f,100}$ = $w_{PE}(\Delta H_{f(100),PE})$ + $w_{PVOH}(\Delta H_{f(100),PVOH})$].[43] [e]Determined by fitting peaks to a Gaussian model to determine area under crystalline peaks and amorphous halo. χ_c = area of crystalline peaks/(area of crystalline peaks + area of amorphous halo). [f]Determined using DMTA by taking the maximum of tan(δ) in the region between 25 and 100 °C. [g]Determined by DSC of melt-pressed and quenched film from the first heating cycle (10 °C·min^{-1}).

crystallinity when comparing PH3OHCOE and PH5OHCOE, we prepared a lower molar mass derivative of PH3OHCOE by polymerizing 3AcCOE with *cis*-4-octene as a chain-transfer agent, targeting the molar mass of PH5OHCOE (78 kg·mol^{-1}). This was followed by hydrogenation and deacylation. Due to previously mentioned column interactions between PH3OHCOE and the HFIP-SEC, molar mass was determined at the previous step (PH3AcCOE) by THF-SEC. The modified PH3OHCOE polymer had an estimated M_n value of 71 kg·mol^{-1} and a $Đ$ value of 1.4. This polymer was cast into a thin film from HFIP and thermally annealed in the same manner as the previous films, then analyzed by DSC to compare ΔH_m values (Figure S34, Table S2). The T_m was 149 °C and the ΔH_m was 109 J·g^{-1}, still considerably higher than that of PH5OHCOE. This is consistent with regioregularity of this polymer being the main factor associated with higher levels of crystallinity (χ_c) and a higher melting point.

Wide-Angle X-Ray Scattering. 1D WAXS was also used to explore the structure and χ_c for the solvent-cast samples (Figure 4). All three samples showed relatively sharp peaks, consistent with their semicrystalline nature. After integrating the amorphous halo and the crystalline peaks, χ_c can be estimated from the ratio of crystalline area to the total area of all peaks.[40,41] Peak fitting software was used to deconvolute the crystalline peaks and amorphous contributions with Gaussian fits. These were then integrated for χ_c calculations (Figures S35–S40). While χ_c values matched closely for PH3OHCOE and EVOH-44 to values obtained by DSC, PH5OHCOE had a higher χ_c value from WAXS, although still lower than PH3OHCOE.

Differences in scattering patterns were also observed between the different samples (Figure 4). Previous literature reported that EVOH copolymers with higher vinyl alcohol content exhibit a monoclinic crystal structure, while those with higher ethylene content exhibit an orthorhombic crystal

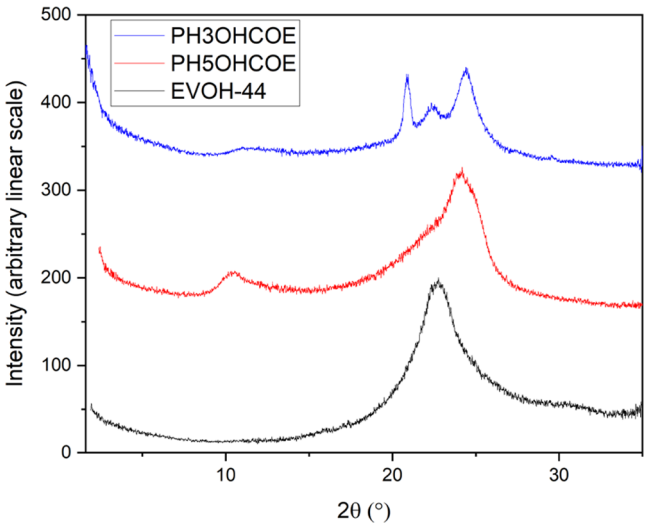

Figure 4. 1D WAXS of commercial EVOH-44 (bottom, black), PH5OHCOE (middle, red), and PH3OHCOE (top, blue). Traces shifted vertically for clarity.

structure. However, a pseudohexagonal crystal structure has been observed in a transition region between the copolymer compositions that define the monoclinic and orthorhombic regions and typically exhibits fewer X-ray reflections.[44,45] The exact copolymer composition for this transition region has been reported to be 20–60 mol % vinyl alcohol content in one publication[45] and 14–27 mol % vinyl alcohol content in another,[44] although processing conditions will also impact the observed crystal structure.[46] All being equal, the ROMP-derived polymers in this study should lie in the pseudohexagonal region with 25 mol % vinyl alcohol content, which has just one strong crystalline peak in this 2θ range at 24° (d = 4.3 Å).[44] However, the PH3OHCOE sample showed several sharp WAXS peaks, more than expected as compared to typical pseudohexagonal EVOH samples. Although the exact crystal structure for these polymers was not determined independently, the observed scattering peaks can be compared to literature values to obtain more information.

Both PH3OHCOE and PH5OHCOE have peaks at 11.1° (d = 8.7 Å) and 10.5° (d = 9.8 Å), respectively, where these d-spacings both roughly correspond to the distance between hydroxyl groups (~10 Å) along the planar zig-zag chain (Figure S44). This also correlates well to the [100] plane of the monoclinic unit cell for EVOH.[45] By setting this peak to the [100] plane, theoretical monoclinic reflections can be compared to the experimental data (Figures S46 and S47). Although the perfect agreement was not achieved, PH3OHCOE had a very similar experimental 1D WAXS pattern to a monoclinic EVOH copolymer with 62.9 mol % vinyl alcohol content.[45] PH5OHOE only has one additional reflection at 24.2° (d = 4.3 Å), consistent with more pseudohexagonal character and less monoclinic character compared to PH3OHCOE. Based on the breadth of the reflections, the largest scattering peak for PH5OHCOE could include peaks associated with both monoclinic and pseudohexagonal structures. This could explain the discrepancy between χ_c values obtained from DSC and WAXS for PH5OHCOE; such complicated patterns can render peak deconvolution less precise. Additionally, PH3OHCOE and PH5OHCOE were compared to literature reflections for orthorhombic EVOH, but the peaks were not consistent with an orthorhombic

https://doi.org/10.1021/acsapm.2c01918
ACS Appl. Polym. Mater. 2023, 5, 1828–1836

structure (Figures S48 and S49). Chain alignment by uniaxial stretching of thin films above their T_g was attempted to further elucidate information about the crystal structure, but no significant changes in the WAXS data were observed.

To form a monoclinic crystal structure in EVOH polymers, regular hydrogen bonding between −OH groups from different chains is necessary.[47] High vinyl alcohol content ensures that this is possible in statistical copolymers, but as vinyl alcohol content decreases, the number of nonhydrogen-bonded −OH groups increases.[48,49] We hypothesize that the precise and regular structure of PH3OHCOE, where −OH groups are located every eight carbons along the backbone, allows for more hydrogen bonds to be formed and for a monoclinic crystal structure to be observed at this relatively low vinyl alcohol content. Interestingly, the commercial EVOH-44 appears to fit the pseudohexagonal structure, despite having higher vinyl alcohol content.

Mechanical Properties. Understanding the mechanical behavior of these polymers is important to determine processing parameters and potential applications. To analyze mechanical behavior, dynamic mechanical thermal analysis (DMTA) was used to observe changes in the extensional moduli of the solvent-cast films over a temperature range (Figure 5). In all three traces, two thermal transitions were

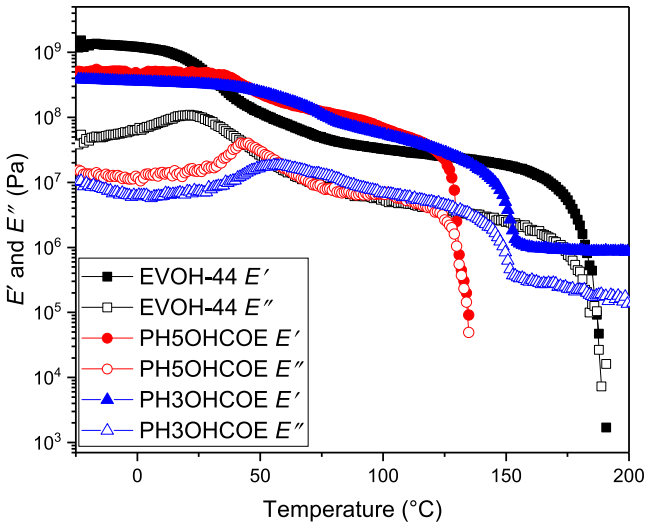

Figure 5. Extensional DMTA (5 °C·min^{-1}, 0.1% strain, 1.0 Hz) of commercial EVOH-44 (black square), PH5OHCOE (red circle), and PH3OHCOE (blue triangle). Filled symbols represent storage modulus (E'), and open symbols represent loss modulus (E'').

observed: T_g and T_m. T_g is shown by an increase in E'' (loss modulus), a drop in E' (storage modulus), and a maximum in tan(δ). Below T_g, EVOH-44 has the highest E', followed by PH5OHCOE, then PH3OHCOE, indicating a higher material stiffness at room temperature for EVOH-44. The opposite trend was observed for the value of T_g, where EVOH-44 has the lowest T_g, followed by PH5OHCOE, then PH3OHCOE. However, the values are significantly lower than the values obtained from DSC (Figure S82, Table S5), although the trend remains the same. Above T_g, PH3OHCOE and PH5OHCOE have similar moduli values, but the value of E' for EVOH-44 drops below that of the synthesized polymers, indicating a softer material above T_g. The second transition, T_m, occurs with a decrease in both moduli, with E' crossing below E''. The T_m values match well to DSC results for all three polymers; however, the E' and E'' of PH3OHCOE decrease but never crossed up to the highest temperature probed. This effect was also observed by shear rheology above T_m (Figures S54−S67). This behavior could indicate material cross-linking; however, the material was still soluble in HFIP after the experiment when stopped at 170 °C. DSC analysis did show an exotherm, potentially due to a putative cross-linking reaction, at a higher temperature of 200 °C (Figure S68). However, this reaction occurs above the temperature range for these DMTA experiments. This high-temperature exotherm can be mitigated through the addition of antioxidant butylated hydroxytoluene (BHT) (Figure S69). To confirm the sample was not undergoing a cross-linking reaction, the DMTA experiment was repeated with and without BHT (Figure S70), but no difference was observed.

To determine if molar mass was affecting this behavior at T_m, a molar mass series of PH3OHCOE was synthesized (Table S3), processed by solvent-casting, then compared using the same DMTA experiment (Figure S71). A moduli crossover was observed in lower molar mass samples (20 and 71 kg·mol^{-1}) but not in higher molar mass samples (119 and 215 kg·mol^{-1}). Variable-temperature WAXS was then used to determine if there was any ordered structure (e.g., liquid crystallinity) in the polymer melt that could be responsible for the lack of moduli crossover at T_m (Figures S72−S78). All four polymers showed the disappearance of crystalline peaks after their respective T_m, leaving only peaks from the Kapton used to mount the sample. We also looked to polar optical microscopy (POM) to observe the polymers from 25 to 225 °C (Supporting Information Videos). While both PH3OHCOE and PH5OHCOE show expected birefringence from 25 °C to their respective T_m, PH3OHCOE continues to exhibit birefringence above 200 °C. This effect also appears to be molar mass dependent, where the birefringent areas of the 20 and 71 kg·mol^{-1} polymers disappear at their T_m. Intermolecular hydrogen bonding can have a drastic effect on the rheological properties of polymers, typically increasing the temperature at which flow is observed.[50] As discussed previously, the WAXS data support that the regioregularity of PH3OHCOE allows for high hydrogen-bonding ability of −OH groups and a more monoclinic-type crystal structure. This high extent of hydrogen bonding could lead to the lack of flow at the T_m and continued birefringence above T_m in POM. While the material should flow at a higher temperature (∼215 °C based on POM) in this case, the putative high-temperature cross-linking reaction observed in Figure S68 could prevent the material from reaching terminal flow.

Tensile testing results for the solvent-cast films are shown in Figure 6 and summarized in Table S4. While the molar masses for these polymers are different, we hypothesize changes in molecular structure impact the properties more significantly than the changes in molar mass above a critical value. Young's modulus (E) was highest for EVOH-44 at 1.5 GPa, followed by PH5OHCOE at 0.63 GPa, then PH3OHCOE (215 kg·mol^{-1}) at 0.28 GPa. These data corroborate the trend in E' observed by DMTA at room temperature. Although an increase in crystallinity can result in an increase in stiffness and modulus, changes in the crystal structure, morphology, and copolymer composition also affect mechanical properties.[51−53] PH3OHCOE has a lower toughness value of 0.4 MJ·m^{-3} and a lower stress-at-break (σ_b) of 3.7 MPa, compared to 0.7 MJ·m^{-3} and 18 MPa for EVOH-44, respectively. Both samples exhibit brittle behavior upon breaking. However, the strain-at-break

https://doi.org/10.1021/acsapm.2c01918
ACS Appl. Polym. Mater. 2023, 5, 1828−1836

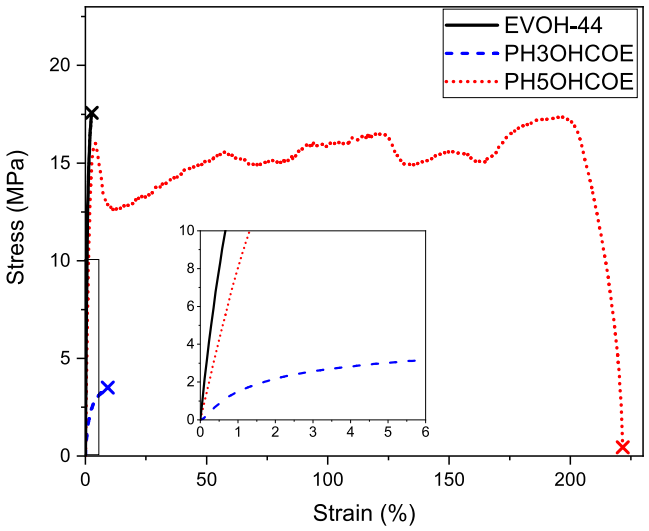

Figure 6. Tensile testing (1 mm·min^{-1}) of commercial EVOH-44 (black line), PH5OHCOE (red dot), and PH3OHCOE (blue dash). X marks material failure. The low-strain region is expanded for easier Young's modulus comparison.

(ε_b) is slightly lower for EVOH-44 at 4.1% compared to PH3OHCOE at 9.9%. Interestingly, PH5OHCOE exhibits ductile behavior, unlike the other two samples. A yield point was observed at 3.6% strain and 12 MPa. PH5OHCOE also exhibited a much higher ε_b of 260%, leading to a significantly higher toughness of 33 MJ·m^{-3} compared to EVOH-44 and PH3OHCOE. Despite these characteristics, this sample slowly tore in the grips, leading to a σ_b of 4.6 MPa, similar to that for PH3OHCOE.

Barrier Testing. To determine the oxygen permeability (P_{O2}) of the polymer samples, the oxygen transmission rate was measured using oxygen as the test gas and nitrogen as the carrier gas at 0% relative humidity. During gas barrier measurements, small pinhole defects in polymer films can artificially raise permeability values. To remove these defects, we briefly processed the solvent-cast film samples in a melt-press 15 °C above their respective T_m values at 15,000 psig (103 MPa) for 10 s. The resulting films were then quenched in a water-cooled press to cool to room temperature and annealed at 85 °C for 2 h. The thermal properties of these polymers are shown in Figure S82 and Table S5, where the crystallinity of EVOH-44 surpasses that of the ROMP-derived polymers, affirming density results in Table 1. Additionally, a T_g is apparent in the heating trace of these samples (Table 2).

Permeability was calculated from the transmission rate by accounting for film thickness and gas pressure. The results of this test are shown in Figure 7a and Table S6 and list the average of two measurements per sample type. With the highest χ_c, EVOH-44 showed the lowest P_{O2} of 0.24 cc·mil·(100 in^2·day·atm)$^{-1}$. This is consistent with previous permeability measurements for EVOH copolymers.[54] For the ROMP-based polymers, PH3OHCOE (215 kg·mol^{-1}) exhibits a lower P_{O2} of 11 cc·mil·(100 in^2·day·atm)$^{-1}$ compared to PH5OHCOE at 36 cc·mil·(100 in^2·day·atm)$^{-1}$. PH3OHCOE has a higher χ_c and T_g compared to PH5OHCOE. Additionally, the increased hydrogen bonding indicated by WAXS and DMTA can also decrease the fractional free volume in PH3OHCOE. The P_{O2} difference between these polymers is likely due to the combined effect of enhanced crystallinity and lower free volume in the regioregular polymer.

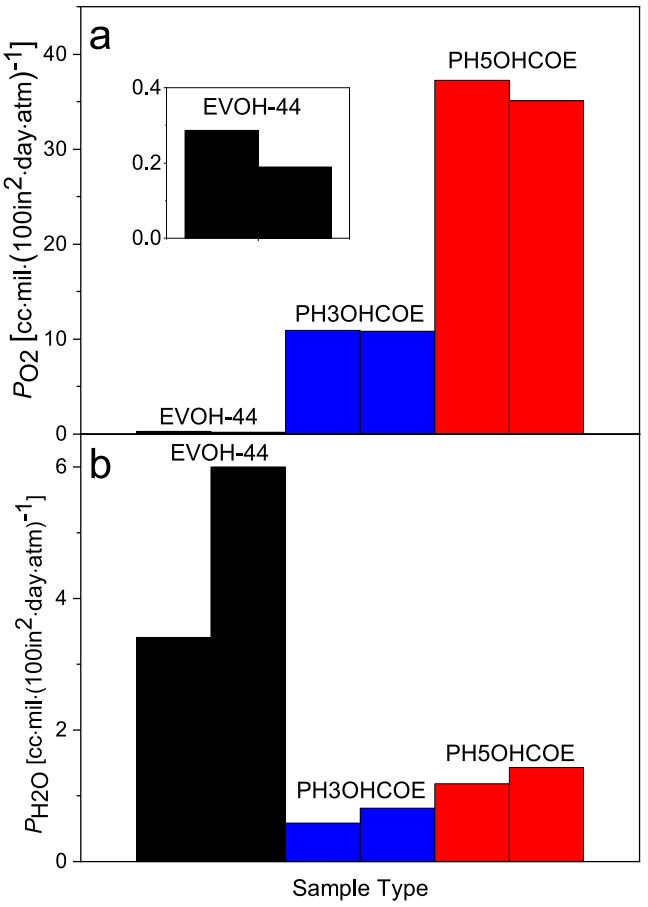

Figure 7. P_{O2} (a) and P_{H2O} (b) for EVOH-44 (left, black), PH3OHCOE (middle, blue), and PH5OHCOE (right, red). Two trials were tested per sample type; each sample type has two bars representing these two trials.

The water permeability (P_{H2O}) was also measured from the water vapor transmission rate under 90% relative humidity accounting for film thickness (Figure 7b, Table S6), where each value is an average of two measurements per sample type. In this case, samples were melt-pressed from powder at 15 °C above their respective T_m under 15,000 psig for 3 min followed by cooling to room temperature in the press at a rate of 25 °C·min^{-1}. The samples were then annealed at 85 °C for 2 h. PH3OHCOE with a lower molar mass (71 kg/mol) was used due to low sample availability. As expected, EVOH-44 has the highest P_{H2O} of 4.7 cc·mil·(100 in^2·day·atm)$^{-1}$ due to its higher vinyl alcohol content (water is more soluble in materials with more polar hydroxyl groups). While PH3OHCOE and PH5OHCOE have more similar P_{H2O} values, PH3OHCOE still has a lower average P_{H2O} of 0.7 cc·mil·(100 in^2·day·atm)$^{-1}$, which was a factor of about 6 lower than EVOH-44. We attribute this to similar factors as those stated above (higher χ_c, T_g, and intermolecular interactions).

CONCLUSIONS

Regioregular PH3OHCOE and regiorandom PH5OHCOE were synthesized by ROMP of their respective monomers, followed by hydrogenation and deacylation. Although molar mass discrepancies are present between these samples, we determined that at high values, molar mass did not influence ΔH_m. By DSC, PH3OHCOE had the highest χ_c, followed by PH5OHCOE, then commercial EVOH-44 after solvent-

https://doi.org/10.1021/acsapm.2c01918
ACS Appl. Polym. Mater. 2023, 5, 1828−1836

casting. WAXS generally showed similar values of χ_c and that PH3OHCOE had more monoclinic crystal structure character compared to PH5OHCOE. Although DMTA showed T_g and T_m transitions for all polymers, PH3OHCOE did not show moduli crossover at T_m at high molar masses (>100 kg·mol^{-1}). This effect was attributed to the high hydrogen-bonding ability from regular placement of −OH groups along the backbone. Tensile testing confirmed the moduli exhibited by DMTA, with a decreasing trend in moduli from EVOH-44, PH5OHCOE, and then PH3OHCOE. While EVOH-44 and PH3OHCOE exhibit brittle failure at low strain, PH5OHCOE is a ductile material with a yield point, high toughness, and high strain at break. Finally, barrier testing measurements confirmed our hypothesis that regioregularity decreases P_{O2}, with this value being lower for PH3OHCOE than PH5OHCOE. EVOH-44 still exhibits the lowest P_{O2} due to its higher vinyl alcohol content and higher χ_c after melt-pressing. However, EVOH-44 has a much higher P_{H2O} compared to PH3OHCOE and PH5OHCOE. These results demonstrate that through increased structural regularity, P_{O2} can be decreased in EVOH films with low vinyl alcohol content while maintaining low P_{H2O}. Further structural improvements could lead to high-performing single-layer EVOH barrier materials.

■ ASSOCIATED CONTENT

Data Availability Statement

The data that support the findings of this study are openly available in the Data Repository at the University of Minnesota (DRUM) at the following location: https://doi.org/10.13020/vb1d-5r77.

Supporting Information

The Supporting Information is available free of charge at https://pubs.acs.org/doi/10.1021/acsapm.2c01918.

Experimental details, NMR spectra, NMR, and SEC kinetics data; TGA traces, additional DSC traces, thermal and molar mass data for PH3OHCOE with varying molar masses; additional 1D and 2D scattering data and figures; additional rheology and tensile data; and variable-temperature WAXS data (PDF)
PH3OHCOE-20K-heat-cool-heat (MP4)
PH3OHCOE-70K-heat-cool-heat (MP4)
PH3OHCOE-119K-heat (MP4)
PH3OHCOE-215K-heat (MP4)
PH5OHCOE-heat (MP4)

■ AUTHOR INFORMATION

Corresponding Author

Marc A. Hillmyer − *Department of Chemistry, University of Minnesota, Minneapolis, Minnesota 55455, United States;* orcid.org/0000-0001-8255-3853; Email: hillmyer@umn.edu

Author

Claire E. Dingwell − *Department of Chemistry, University of Minnesota, Minneapolis, Minnesota 55455, United States*

Complete contact information is available at: https://pubs.acs.org/10.1021/acsapm.2c01918

Author Contributions

C.E.D. and M.A.H. contributed to project conception, experimental approach, and manuscript preparation. C.E.D. performed described experiments unless specified otherwise in the acknowledgments.

Notes

The authors declare no competing financial interest.

■ ACKNOWLEDGMENTS

The authors thank The Dow Chemical Company for partial financial support of this research. The authors thank Dr. Jeff Munro, Dr. Colin Li Pi Shan, Dr. Thomas Peterson, and Dr. Christopher Thurber for input. All rheology was carried out in the College of Science and Engineering Polymer Characterization Facility, University of Minnesota, which has received capital equipment funding from the NSF through MRSEC. WAXS was carried out in the Characterization Facility, University of Minnesota, which receives partial support from the NSF through MRSEC. The authors would like to thank Dr. Geoffrey Rojas (UMN Charfac) and Dr. Victor Young (UMN X-ray Crystallographic Laboratory) for conducting room-temperature WAXS experiments and Donald Massey for performing barrier measurements in the Center for Flexible Packaging, Clemson University. The authors would also like to thank Yoon-Jung Jang, Dr. Stephanie Liffland, and Dr. Caitlin Sample for helpful discussion.

■ REFERENCES

(1) López-Rubio, A.; Almenar, E.; Hernandez-Muñoz, P.; Lagarón, J. M.; Catalá, R.; Gavara, R. Overview of Active Polymer-Based Packaging Technologies for Food Applications. *Food Rev. Int.* **2004**, *20*, 357−387.
(2) Hovorka, S. W.; Schöneich, C. Oxidative Degradation of Pharmaceuticals: Theory, Mechanisms and Inhibition. *J. Pharm. Sci.* **2001**, *90*, 253−269.
(3) Koros, W. J. Barrier Polymers and Structures: Overview. In *Barrier Polymers and Structures*; ACS Symposium Series; American Chemical Society, 1990; Vol. *423*, pp 1−21.
(4) Blackwell, A. L. Ethylene Vinyl Alcohol Resins as a Barrier Material in Multi-Layer Packages. *J. Plast. Film Sheeting* **1985**, *1*, 205−214.
(5) Ketels, H.; Beulen, J.; Van der Velden, G. Tacticity, Sequence Distribution, Anomalous Linkages, and Alkyl Chain Branching in Ethylene-Vinyl Alcohol Copolymers as Studied by Proton and Carbon-13 NMR. *Macromolecules* **1988**, *21*, 2032−2037.
(6) Holland, B. J.; Hay, J. N. The Thermal Degradation of Poly(Vinyl Alcohol). *Polymer* **2001**, *42*, 6775−6783.
(7) Mokwena, K. K.; Tang, J. Ethylene Vinyl Alcohol: A Review of Barrier Properties for Packaging Shelf Stable Foods. *Crit. Rev. Food Sci. Nutr.* **2012**, *52*, 640−650.
(8) Kuraray. *Gas Barrier Properties of Resins*; 110; Houston, TX; pp 1−12.
(9) EVAL Resins: The Better Barrier for Food Applications, 2015.
(10) Zhang, Z.; Britt, I. J.; Tung, M. A. Permeation of Oxygen and Water Vapor through EVOH Films as Influenced by Relative Humidity. *J. Appl. Polym. Sci.* **2001**, *82*, 1866−1872.
(11) Muramatsu, M.; Okura, M.; Kuboyama, K.; Ougizawa, T.; Yamamoto, T.; Nishihara, Y.; Saito, Y.; Ito, K.; Hirata, K.; Kobayashi, Y. Oxygen Permeability and Free Volume Hole Size in Ethylene−Vinyl Alcohol Copolymer Film: Temperature and Humidity Dependence. *Radiat. Phys. Chem.* **2003**, *68*, 561−564.
(12) Graham, T. On the Absorption and Dialytic Separation of Gases by Colloid Septa. *London, Edinburgh Dublin Philos. Mag. J. Sci.* **1866**, *32*, 401−420.
(13) Ghosal, K.; Freeman, B. D. Gas Separation Using Polymer Membranes: An Overview. *Polym. Adv. Technol.* **1994**, *5*, 673−697.
(14) Salame, M.; Steingiser, S. Barrier Polymers. *Polym.-Plast. Technol. Eng.* **1977**, *8*, 155−175.

(15) Lagaron, J. M.; Catalá, R.; Gavara, R. Structural Characteristics Defining High Barrier Properties in Polymeric Materials. *Mater. Sci. Technol.* **2004**, *20*, 1−7.
(16) Michaels, A. S.; Vieth, W. R.; Barrie, J. A. Diffusion of Gases in Polyethylene Terephthalate. *J. Appl. Phys.* **1963**, *34*, 13−20.
(17) Maes, C.; Luyten, W.; Herremans, G.; Peeters, R.; Carleer, R.; Buntinx, M. Recent Updates on the Barrier Properties of Ethylene Vinyl Alcohol Copolymer (EVOH): A Review. *Polym. Rev.* **2018**, *58*, 209−246.
(18) Ito, K.; Saito, Y.; Yamamoto, T.; Ujihira, Y.; Nomura, K. Correlation Study between Oxygen Permeability and Free Volume of Ethylene−Vinyl Alcohol Copolymer through Positronium Lifetime Measurement. *Macromolecules* **2001**, *34*, 6153−6155.
(19) Hodge, R. M.; Edward, G. H.; Simon, G. P. Water Absorption and States of Water in Semicrystalline Poly(Vinyl Alcohol) Films. *Polymer* **1996**, *37*, 1371−1376.
(20) Hiemenz, P. C.; Lodge, T. P. *Polymer Chemistry*, 2nd ed.; CRC Press, 2007; pp 1−608.
(21) Grubbs, R. H. *Handbook of Metathesis*; Wiley-VCH, 2003; Vol. 3, pp 1−424.
(22) Martinez, H.; Ren, N.; Matta, M. E.; Hillmyer, M. A. Ring-Opening Metathesis Polymerization of 8-Membered Cyclic Olefins. *Polym. Chem.* **2014**, *5*, 3507−3532.
(23) Ramakrishnan, S.; Chung, T. C. Poly(5-Hydroxyoctenylene) and Its Derivatives: Synthesis via Metathesis Polymerization of an Organoborane Monomer. *Macromolecules* **1990**, *23*, 4519−4524.
(24) Hillmyer, M. A.; Laredo, W. R.; Grubbs, R. H. Ring-Opening Metathesis Polymerization of Functionalized Cyclooctenes by a Ruthenium-Based Metathesis Catalyst. *Macromolecules* **1995**, *28*, 6311−6316.
(25) Ramakrishnan, S. Well-Defined Ethylene-Vinyl Alcohol Copolymers via Hydroboration: Control of Composition and Distribution of the Hydroxyl Groups on the Polymer Backbone. *Macromolecules* **1991**, *24*, 3753−3759.
(26) Scherman, O. A.; Walker, R.; Grubbs, R. H. Synthesis and Characterization of Stereoregular Ethylene-Vinyl Alcohol Copolymers Made by Ring-Opening Metathesis Polymerization. *Macromolecules* **2005**, *38*, 9009−9014.
(27) Scherman, O. A.; Kim, H. M.; Grubbs, R. H. Synthesis of Well-Defined Poly[(Vinyl Alcohol)$_2$-*alt*-Methylene] via Ring-Opening Metathesis Polymerization. *Macromolecules* **2002**, *35*, 5366−5371.
(28) Tuba, R.; Al-Hashimi, M.; Bazzi, H. S.; Grubbs, R. H. One-Pot Synthesis of Poly(Vinyl Alcohol) (PVA) Copolymers via Ruthenium Catalyzed Equilibrium Ring-Opening Metathesis Polymerization of Hydroxyl Functionalized Cyclopentene. *Macromolecules* **2014**, *47*, 8190−8195.
(29) Guillory, G. A.; Marxsen, S. F.; Alamo, R. G.; Kennemur, J. G. Precise Isotactic or Atactic Pendant Alcohols on a Polyethylene Backbone at Every Fifth Carbon: Synthesis, Crystallization, and Thermal Properties. *Macromolecules* **2022**, *55*, 6841−6851.
(30) Kobayashi, S.; Pitet, L. M.; Hillmyer, M. A. Regio- and Stereoselective Ring-Opening Metathesis Polymerization of 3-Substituted Cyclooctenes. *J. Am. Chem. Soc.* **2011**, *133*, 5794−5797.
(31) Zhang, J.; Matta, M. E.; Hillmyer, M. A. Synthesis of Sequence-Specific Vinyl Copolymers by Regioselective ROMP of Multiply Substituted Cyclooctenes. *ACS Macro Lett.* **2012**, *1*, 1383−1387.
(32) Martinez, H.; Miró, P.; Charbonneau, P.; Hillmyer, M. A.; Cramer, C. J. Selectivity in Ring-Opening Metathesis Polymerization of *Z*-Cyclooctenes Catalyzed by a Second-Generation Grubbs Catalyst. *ACS Catal.* **2012**, *2*, 2547−2556.
(33) Zhang, J.; Matta, M. E.; Martinez, H.; Hillmyer, M. A. Precision Vinyl Acetate/Ethylene (VAE) Copolymers by ROMP of Acetoxy-Substituted Cyclic Alkenes. *Macromolecules* **2013**, *46*, 2535−2543.
(34) Walker, T. W.; Frelka, N.; Shen, Z.; Chew, A. K.; Banick, J.; Grey, S.; Kim, M. S.; Dumesic, J. A.; Van Lehn, R. C.; Huber, G. W. Recycling of Multilayer Plastic Packaging Materials by Solvent-Targeted Recovery and Precipitation. *Sci. Adv.* **2020**, *6*, No. eaba7599.
(35) Radlauer, M. R.; Matta, M. E.; Hillmyer, M. A. Regioselective Cross Metathesis for Block and Heterotelechelic Polymer Synthesis. *Polym. Chem.* **2016**, *7*, 6269−6278.
(36) Martinez, H.; Zhang, J.; Kobayashi, S.; Xu, Y.; Pitet, L. M.; Matta, M. E.; Hillmyer, M. A. Functionalized Regio-Regular Linear Polyethylenes from the ROMP of 3-Substituted Cyclooctenes. *Appl. Petrochem. Res.* **2015**, *5*, 19−25.
(37) Wang, Y.; Hillmyer, M. A. Hydroxy-Telechelic Poly(Ethylene-*Co*-Isobutylene) as a Soft Segment for Thermoplastic Polyurethanes. *Polym. Chem.* **2015**, *6*, 6806−6811.
(38) Kholodovych, V.; Welsh, W. J. Densities of Amorphous and Crystalline Polymers. In *Physical Properties of Polymers Handbook*; Mark, J. E., Ed.; Springer: New York, NY, 2007; pp 611−617.
(39) Mandelkern, L.; Allou, A. L.; Gopalan, M. R. Enthalpy of Fusion of Linear Polyethylene. *J. Phys. Chem. A* **1968**, *72*, 309−318.
(40) Challa, G.; Hermans, P. H.; Weidinger, A. On the Determination of the Crystalline Fraction in Isotactic Polystyrene from X-Ray Diffraction. *Makromol. Chem.* **1962**, *56*, 169−178.
(41) Rabiej, S.; Wlochowicz, A. SAXS and WAXS Investigations of the Crystallinity in Polymers. *Angew. Makromol. Chem.* **1990**, *175*, 81−97.
(42) Blaine, R. L. Thermal Applications Note, **2002**; 1−2.
(43) Faisant, J. B.; Aït-Kadi, A.; Bousmina, M.; Deschênes, L. Morphology, Thermomechanical and Barrier Properties of Polypropylene-Ethylene Vinyl Alcohol Blends. *Polymer* **1998**, *39*, 533−545.
(44) Takahashi, M.; Tashiro, K.; Amiya, S. Crystal Structure of Ethylene−Vinyl Alcohol Copolymers. *Macromolecules* **1999**, *32*, 5860−5871.
(45) Matsumoto, T.; Nakamae, K.; Ogoshi, N.; Kawasoe, M.; Oka, H. The Crystallinity of Ethylene-Vinyl Alcohol Copolymers. *Kobunshi Kagaku* **1971**, *28*, 610−617.
(46) Cerrada, M. L.; Pérez, E.; Pereña, J. M.; Benavente, R. Wide-Angle X-Ray Diffraction Study of the Phase Behavior of Vinyl Alcohol−Ethylene Copolymers. *Macromolecules* **1998**, *31*, 2559−2564.
(47) Bunn, C. W. Crystal Structure of Polyvinyl Alcohol. *Nature* **1948**, *161*, 929−930.
(48) Akahane, T.; Kazusa, Y.; Nakayasu, H. An Investigation on the Hydrogen Bonding of Ethylene-Vinyl Alcohol Copolymers by Near-Infrared Spectra. *Kobunshi Ronbunshu* **1980**, *37*, 383−387.
(49) Xu, W.; Asai, S.; Sumita, M. Spectroscopic Study of Ethylene Vinyl Alcohol Copolymer and Poly (Vinyl Alcohol). *Sen'i Gakkaishi* **1997**, *53*, 174−182.
(50) Folmer, B. J. B.; Sijbesma, R. P.; Versteegen, R. M.; van der Rijt, J. A. J.; Meijer, E. W. Supramolecular Polymer Materials: Chain Extension of Telechelic Polymers Using a Reactive Hydrogen-Bonding Synthon. *Adv. Mater.* **2000**, *12*, 874−878.
(51) Phillips, P. J.; Patel, J. The Influence of Morphology on the Tensile Properties of Polyethylenes. *Polym. Eng. Sci.* **1978**, *18*, 943−950.
(52) Porter, R. S.; Southern, J. H.; Weeks, N. Polymer Modulus and Morphology: The Tensile Properties of Polyethylene. *Polym. Eng. Sci.* **1975**, *15*, 213−218.
(53) Nakamae, K.; Kameyama, M.; Matsumoto, T. Elastic moduli of the crystalline regions in the direction perpendicular to the chain axis of ethylene-vinyl alcohol copolymers. *Polym. Eng. Sci.* **1979**, *19*, 572−578.
(54) Ito, K.; Hong-ling, L.; Saito, Y.; Yamamoto, T.; Nishihara, Y.; Ujihira, Y.; Nomura, K. Free-Volume Study of Ethylene - Vinyl Alcohol Copolymer Evaluated through Positronium Lifetime Measurement. *J. Radioanal. Nucl. Chem.* **2003**, *255*, 437−441.

https://doi.org/10.1021/acsapm.2c01918
ACS Appl. Polym. Mater. 2023, 5, 1828−1836